NUMERICAL SIMULATIONS OF ROTATING SUNSPOTS

G. J. J. Botha[1], A. M. Rucklidge[1], F. H. Busse[2], and N. E. Hurlburt[3]

[1]*Department of Applied Mathematics, University of Leeds, Leeds, LS2 9JT, UK, Email: gert@maths.leeds.ac.uk; A.M.Rucklidge@leeds.ac.uk*

[2]*Institute of Geophys. Planet. Physics, UCLA, Los Angeles, CA 90024, USA, Email: fbusse@igpp.ucla.edu*

[3]*Lockheed Martin Solar and Astrophysics Laboratory, Organization L9-41 Building 252, Palo Alto, CA 94304, USA, Email: hurlburt@lmsal.com*

ABSTRACT

A numerical model of idealized, axisymmetric, rotating sunspots is presented. The model contains a compressible plasma described by the nonlinear MHD equations, with density and temperature gradients simulating the upper layer of the sun's convection zone. The solution forms a central flux tube in the cylindrical numerical domain, with convection cells pushing the magnetic field to the axis. When the numerical domain is rotated with a constant angular velocity, the umbra rotates as a rigid body while the surrounding convection cells show a swirling, vortical flow. As a result, the azimuthal velocity and magnetic field have their maximum values close to the flux tube, inside the innermost convection cell.

Key words: MHD; convection; Sun: magnetic fields; sunspots.

1. INTRODUCTION

Photospheric white light measurements of rotating sunspots (Brown et al., 2003) show a rotation of up to 200 degrees about the umbral centres over 3 to 5 days. Sunspots have also been observed to undergo damped oscillations (Kučera, 1982). Helioseismic measurements below the surface (Zhao & Kosovichev, 2003) reveal that at a depth of 0 to 12 Mm there is evidence of structural twist. In addition, at a depth of 0 to 5 Mm there exist subsurface horizontal vortical flows, while there are also suggestions that below 9 Mm a vortical flow in the opposite direction to the above may exist.

To investigate the physical processes associated with rotating sunspots, a numerical model of an idealized sunspot is presented. The sunspot is placed in an axisymmetric cylinder with an aspect ratio (radius versus depth) of 3, which is then rotated at a constant angular velocity. The model is described in Sections 2 and 3. Two sets of results are discussed (Sections 4 and 5) that were obtained with different temperature boundary conditions at the bottom of the numerical domain. Finally, the effect of the amplitude of the reference frame's angular velocity is discussed in Section 6.

2. MATHEMATICAL MODEL

The initial temperature and density profiles are

$$T = T_0(1+\theta z), \quad (1)$$

$$\rho = \rho_0(1+\theta z)^m, \quad (2)$$

with the 0 subscript defining the quantity at the top of the box ($z = 0$), θ the initial temperature gradient, and m the polytropic index. Throughout we have used $T_0 = 1$, $\rho_0 = 1$, $\theta = 10$ and $m = 1$. We solve the equations for fully compressible, nonlinear axisymmetric magnetoconvection (Hurlburt & Rucklidge, 2000; Botha et al., 2006):

$$\frac{\partial \rho}{\partial t} = -\nabla\cdot(\mathbf{u}\rho) \quad (3)$$

$$\frac{\partial \mathbf{u}}{\partial t} = -\mathbf{u}\cdot\nabla\mathbf{u} - 2\boldsymbol{\Omega}\times\mathbf{u} + \Omega^2\mathbf{r} + \theta(m+1)\hat{\mathbf{z}} - \frac{1}{\rho}\nabla P + \frac{\sigma K}{\rho}\nabla\cdot\tau - \frac{\sigma\zeta_0 K^2 Q}{\rho}\mathbf{j}\times\mathbf{B} \quad (4)$$

$$\frac{\partial T}{\partial t} = -\mathbf{u}\cdot\nabla T - (\gamma-1)T\nabla\cdot\mathbf{u} + \frac{\gamma K}{\rho}\nabla^2 T + \frac{\sigma K(\gamma-1)}{\rho}\left(\frac{1}{2}\tau:\tau + \zeta_0^2 Q K^2 j^2\right) \quad (5)$$

$$\frac{\partial A_\phi}{\partial t} = (\mathbf{u}\times\mathbf{B})_\phi - \zeta_0 K\mathbf{j}_\phi \quad (6)$$

$$\frac{\partial B_\phi}{\partial t} = \Big[\nabla\times(\mathbf{u}\times\mathbf{B})\Big]_\phi + \zeta_0 K\nabla^2 B_\phi \quad (7)$$

The vector potential A_ϕ gives the r and z components of the magnetic field while the azimuthal component is evolved explicitly, so that the magnetic field is given by

$$\mathbf{B} = \nabla\times(\hat{\phi}A_\phi) + \hat{\phi}B_\phi. \quad (8)$$

The velocity consists of three components, namely $\mathbf{u} = \mathbf{u}(r,\phi,z)$. We also use the auxiliary equations

$$\nabla\cdot\mathbf{B} = 0, \quad (9)$$

$$P = \rho T, \quad (10)$$
$$\mathbf{j} = \nabla \times \mathbf{B}, \quad (11)$$

and the following notation: τ is the rate of strain tensor; γ the ratio of specific heats; σ the Prandtl number; K the dimensionless thermal conductivity; ζ_0 the magnetic diffusivity ratio at $z = 0$; and Q is the Chandrasekhar number. All the other symbols have their usual meaning. The physical quantities are made dimensionless by scaling length $\propto$ depth; time $\propto$ depth / (sound speed at top); and temperature, magnetic field, density, and pressure all proportional to their initial values at the top of the numerical domain. The cylindrical reference frame is rotated in the plane perpendicular to the axis at a constant angular velocity $\mathbf{\Omega} = (d\phi/dt)\hat{\mathbf{z}}$, which results in two additional terms in the Navier-Stokes equation (4).

3. NUMERICAL MODEL

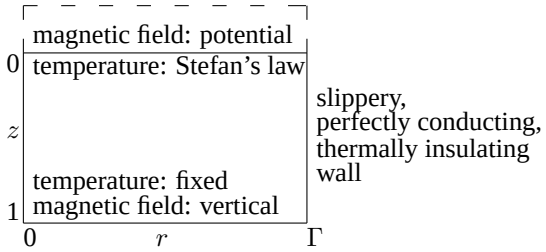

Figure 1. The 2D numerical domain (r, z) of an axisymmetric cylinder with radius Γ and with $z = 0$ at the top of the box.

The computational domain is given in Figure 1. We require that all variables be sufficiently well-behaved at the axis ($r = 0$) and that the differential operators in the PDEs are non-singular. This implies that

$$\frac{\partial \rho}{\partial r} = U_r = \frac{\partial U_z}{\partial r} = A_\phi = B_r = \frac{\partial B_z}{\partial r} = j = \frac{\partial T}{\partial r} = 0. \quad (12)$$

Terms like u/r are evaluated using l'Hôpital's rule. In the numerical simulations we use a fourth-order Bulirsch-Stoer time integration, with sixth-order compact finite differencing (Lele, 1992). The time step was limited by the Courant condition (taking the maximum sound and Alfvén speeds, as well as thermal diffusive limits into account), multiplied by a safety factor of 0.5. A uniform, vertical magnetic field was used as initial condition, and no perturbation was given to the plasma. The time evolution of the plasma is triggered by starting the quiet initial state with the constant angular velocity $|\mathbf{\Omega}|$ of the reference frame.

4. CONVECTION WITH CONSTANT T AT BOTTOM BOUNDARY

These results were obtained with Rayleigh number $R = 10^5$, $Q = 128$, $\Omega = 0.1$, $\sigma = 1$, $\zeta_0 = 0.2$, $\gamma = 5/3$ and $\Gamma = 3$. The solution is shown in Figure 3 when the plasma is almost time independent. All the quantities in the (r, z) plane show no time evolution, while the maxima of the azimuthal quantities are increasing at a very slow rate.

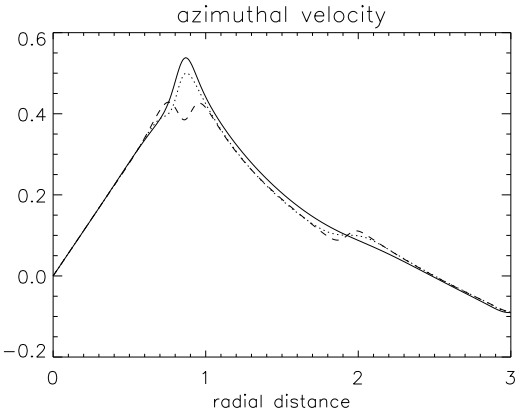

Figure 2. The radial profile of the azimuthal velocity sampled from Figure 3. The solid line is sampled at depth 0.25, the dotted line at depth 0.5, and the dashed line at 0.75.

The convection forces the magnetic flux to the central axis where a strong flux tube forms (Hurlburt & Rucklidge, 2000). Outside the region with strong magnetic field two convection cells form, the inner cell rotating anticlockwise, i.e. at the top towards the magnetic flux tube. Inside the flux tube the density stratification stays as initialized due to the low level of convection there, while outside the flux tube the density shows the effect of the high levels of convection. The radial profile of the azimuthal velocity is presented in Figure 2, taken at different depths from the solution as shown in Figure 3. It shows that the magnetic flux tube rotates as a solid body, so that the maximum azimuthal velocity is reached just outside the magnetic flux tube. Outside the flux tube the velocity decreases in such a way that there exist a swirling vortex around the magnetic flux tube. Figure 2 shows that this is true at all depths in the numerical domain. The azimuthal magnetic field is situated mostly inside the inner convection cell (Figure 3), so that its maximum is close to the magnetic flux tube.

5. CONVECTION WITH CONSTANT $\partial T/\partial Z$ AT BOTTOM BOUNDARY

This result was obtained with the same parameters that were used in the case of a fixed temperature at the bottom boundary (Section 4). The final state of the solution is shown in Figure 4. Again there is little time evolution present, with only the amplitudes of the azimuthal quantities increasing at a very slow rate. The result shows the influence of the choice of boundary conditions on the configuration of the convection cells. The main differ-

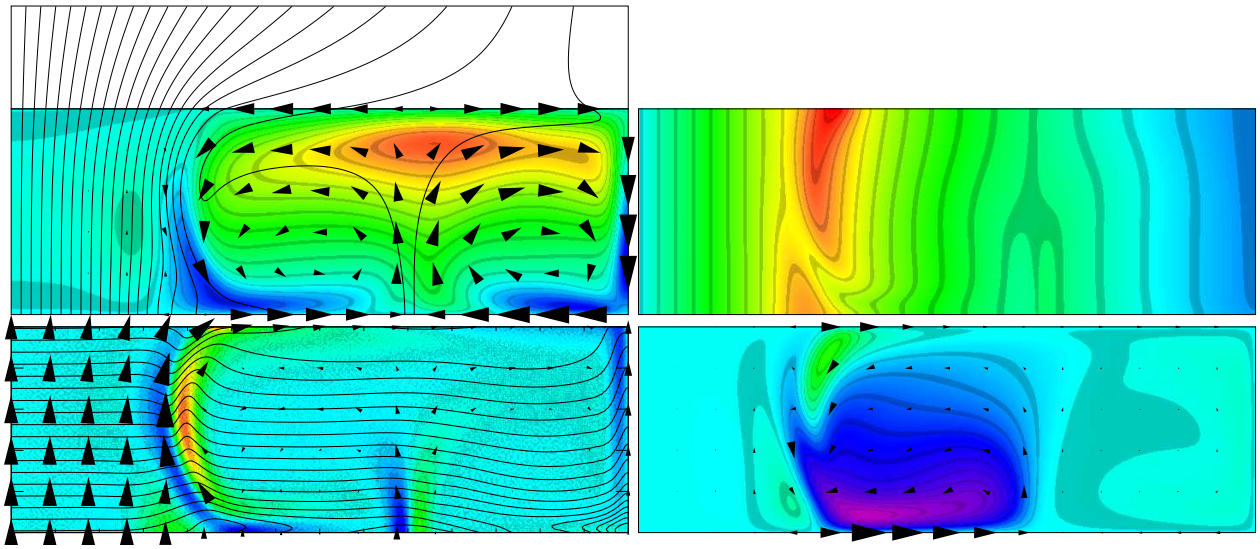

Figure 3. The diagnostic is divided into five boxes. The top box on the left hand side shows the magnetic field lines as calculated for a potential field. The middle layer on the left hand side shows the temperature in colour (blue is cold and red is hot), the velocity field as arrows, and the magnetic field lines as contour lines. The bottom box on the left hand side shows the azimuthal current in colour, the arrows are the magnetic field indicating size and direction, and the contour lines represent the density. The top box on the right hand side shows the azimuthal velocity in colour (blue being negative and red positive), while the bottom box on the right hand side shows the azimuthal magnetic field in colour and the current in the (r, z) plane as arrows. The state of the plasma shown here was obtained with a constant T at the bottom boundary. Its azimuthal velocity shows the rigid rotation of the magnetic flux bundle at the centre of the cylinder, as well as the swirling flow outside the flux tube with the maximum azimuthal flow located in the anticlockwise convection cell next to the flux bundle. The solution shows no time dependence in the (r, z) plane, with the azimuthal quantities increasing very slowly in amplitude.

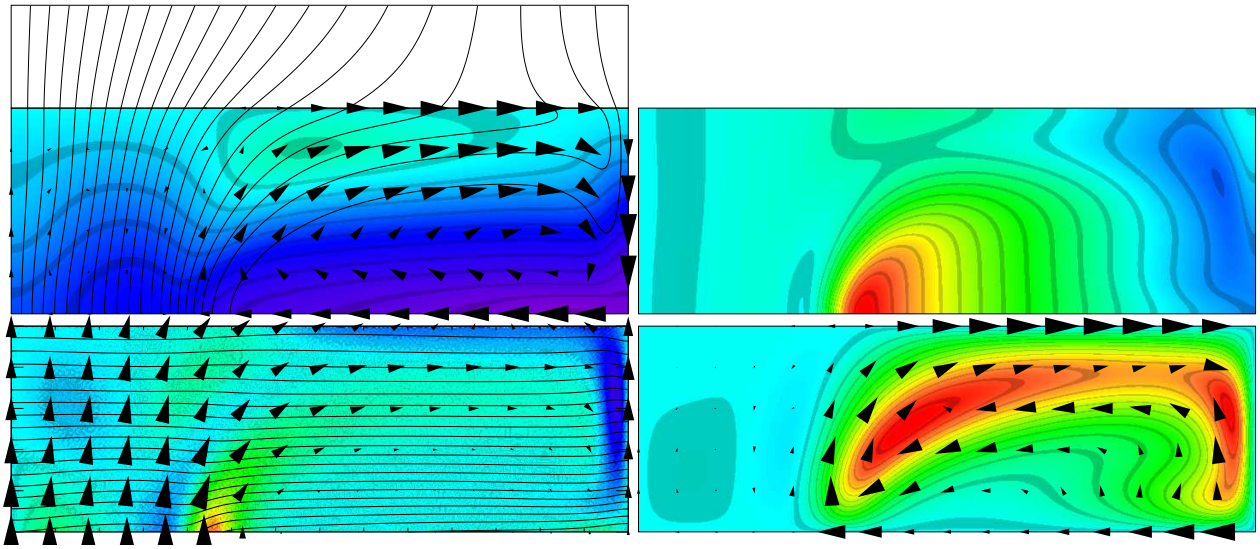

Figure 4. The same diagnostic as was used in Figure 3. This result was obtained with a constant $\partial T/\partial z$ at bottom boundary of the numerical domain, while all the other parameters were kept the same as in Figure 3. The convection cell closest to the magnetic flux bundle has changed direction, resulting in the magnetic flux bundle not being well confined by the convection. The azimuthal quantities show rigid rotation in the flux bundle and a swirling vortical flow in the convection cell. There is no time dependence in the (r, z) plane, with the azimuthal quantities increasing very slowly in amplitude.

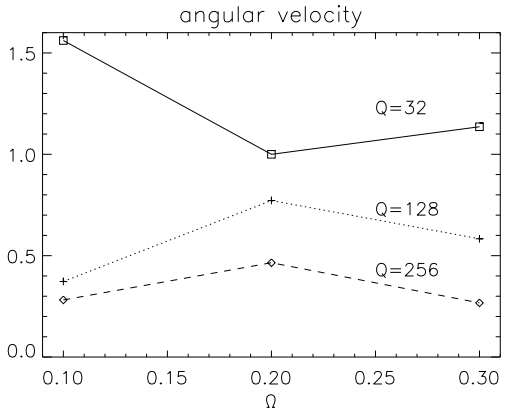

Figure 5. The magnetic flux tube rotates as a solid body. Presented here is the angular velocity of the flux tube as a function of the angular velocity (Ω) of the reference frame, which is constant for any given solution. The measurements were obtained with a constant T at the bottom boundary, as shown in Figure 3.

ence compared to Section 4 (and Figure 3) is a clockwise convection cell that dominates outside the flux tube. As a result, the magnetic flux is not as confined to the central axis as with anticlockwise convection and the azimuthal magnetic field has changed direction.

In spite of the differences between Figures 3 and 4, the magnetic flux tube rotates as a solid body while outside the region with strong magnetic field the azimuthal convection follows a swirling vortical motion as much as the magnetic field configuration allows this to happen. As a result, the maximum of the azimuthal velocity is next to the magnetic flux tube. The azimuthal magnetic component is distributed across the convection cell closest to the magnetic flux bundle, as was the case in Section 5 and Figure 3.

6. RIGID BODY ROTATION

The magnetic flux tube is well defined for simulations with a constant T at the bottom boundary. This flux tube rotates as a solid body around the axis. Although the flux tube is less defined with a constant temperature flux as bottom boundary condition (Figure 4 and Section 5), the regions with strong field still rotate as a solid body. In order to investigate the influence of the size of Ω on the angular velocity of the plasma, the solid body rotation of the magnetic flux tube was monitored for the case of a constant T at the bottom boundary (Figure 3 and Section 4.) Figure 5 shows that there is no direct relation between the angular velocity Ω of the reference frame and the rotation of the magnetic flux tube. It seems that the configuration and vigour of the neighbouring convection cells have a larger influence on the rotation of the magnetic flux tube than the amplitude of Ω. By increasing the size of Ω the strength of convection is increased, but the configuration of the convection cells is dependent on the bottom temperature boundary. An increased Ω also widens the magnetic flux tube at the centre. When it becomes wide enough, convection starts to form inside the flux tube. In contrast, as the magnetic field strength (i.e. Q) increases, the solid body rotation slows down. This can be explained by the fact that a strong magnetic field inhibits convection.

7. SUMMARY

Rotating sunspots were simulated by evolving a plasma in an axisymmetric cylinder, with the cylinder rotating at a constant angular velocity Ω. This Ω drives the velocity components of the plasma through the Navier-Stokes equation (Eq. 4) and as such no initial perturbation of the plasma was needed. Convection cells form in the solution that push the magnetic field towards the central axis of the cylinder to form magnetic flux tubes. These flux tubes display rigid body rotation while the plasma outside the tube experiences a swirling vortical flow. An azimuthal magnetic field forms with a maximum in the convection cell closest to the magnetic flux tube. By increasing the amplitude of Ω, the width of the magnetic flux tube at the central axis increases, which allows convection to form inside the flux tube in the lower local magnetic field strength.

ACKNOWLEDGEMENTS

This work was done with financial support from PPARC and NASA.

REFERENCES

Botha G.J.J, Rucklidge A.M., Hurlburt N.E., 2006, MNRAS, accepted for publication

Brown D.S., Nightingale R.W., Alexander D., Schrijver C.J., Metcalf T.R., Shine R.A., Title A.M., Wolfson C.J., 2003, Solar Physics, 216, 79

Hurlburt N.E., Rucklidge A.M., 2000, MNRAS, 314, 793

Kučera A., 1982, Bulletin of the Astronomical Institutes of Czechoslovakia, 33, 345

Lele S.K., 1992, J. Computational Physics, 103, 16

Zhao J., Kosovichev A.G., 2003, ApJ, 591, 446